Journal of Solid State Chemistry 183 (2010) 2623–2630

Contents lists available at ScienceDirect

Journal of Solid State Chemistry

journal homepage: www.elsevier.com/locate/jssc

Magnetic dilution of the iron sublattice in $CoFe_{2-x}Sc_xO_4$ ($0 \le x \le 1$)

C. Lefevre [a,*], F. Roulland [a], N. Viart [a], J.M. Greneche [b], G. Pourroy [a]

[a] Institut de Physique et Chimie des Matériaux de Strasbourg, UMR 7504 (CNRS–Université de Strasbourg), 23 rue du Loess, BP 43, 67034 Strasbourg, France
[b] Laboratoire de Physique de l'Etat Condensé, UMR 6087 (CNRS–Université du Maine), Avenue Olivier Messiaen, 72085 Le Mans, France

ARTICLE INFO

Article history:
Received 30 April 2010
Received in revised form
23 July 2010
Accepted 1 September 2010
Available online 21 September 2010

Keywords:
Crystalline oxides
X-ray diffraction
Mössbauer spectrometry
Magnetic properties

ABSTRACT

Substitution of Fe for Sc in $CoFe_2O_4$ spinel structure is presented. All $CoFe_{2-x}Sc_xO_4$ compounds crystallize in the spinel type structure (space group $Fd\bar{3}m$). By using X-ray diffraction studies, magnetic measurements and in-field ^{57}Fe Mössbauer spectrometry, the limit of substitution has been determined to be equal to $x=0.56$. An increase in the cell parameter and the strains and a decrease in the apparent crystallites size are observed. For $x > 0.3$, a partial oxidation of cobalt is evidenced and Co^{3+} is stabilized in the structure. A ferromagnetic behavior has been observed for all investigated compounds. As x increases, the Curie temperature and the hyperfine fields decrease. Following the Stephenson model, the diminution of T_C is ascribed to a decrease of the main J_{AB} interaction.

1. Introduction

The spinel structure of general formula AB_2O_4 is complex enough to offer an extraordinary versatility. Remarkable magnetic, electrical and physical properties have been obtained depending on the nature of the different cations and their distribution among the two tetrahedral and octahedral sublattices [1,2]. Spinel phase materials are involved in several technical areas such as magnetic recording, batteries, catalysis or biomedicine [3–7]. For decades, acicular Co-doped maghemite has been used for magnetic recording [8,9]. Both the control of the acicular shape and the Co substitution for Fe contribute to increase the anisotropy and therefore the coercive field. On the contrary, a soft magnetic behavior is observed in NiZn ferrites and Mn powdered ferrites, used as electromagnetic absorbent materials [10,11]. Nowadays, the development of nanosized materials, in multilayers for spintronics or in aqueous suspensions for imaging or hyperthermia treatment of cancer cells opens new fields of applications. This application field requires great effort in chemical synthesis to control the composition, the morphology and the homogeneity of nanostructures, and to investigate and develop new materials. One challenge is to modulate the easy direction of magnetization in the case of multilayers at will. As an example, this could allow designing multilayers in which the adjacent layers would have perpendicular anisotropy directions leading to devices presenting different values of resistivity depending on the applied field direction.

Spinel-type ferrites MFe_2O_4 (M=Fe, Mn, Ni, Co) have a collinear magnetic structure in which the magnetic moment of the (T_d) sites are antiparallel to that of the [O_h] sites [12]. The magnetocrystalline anisotropy constants are rather small for M=Fe, Mn, Ni (at room temperature, $K=-11$, -6.2 and -3 kJ/m^3, respectively) whereas $CoFe_2O_4$ presents a value of K equal to 200 kJ/m^3 coming from a strong Russel–Saunders L-S coupling in Co^{2+} [13]. Due to its anisotropy and reasonable saturation magnetization $M_S=80$ emu/g [14], $CoFe_2O_4$ ferrite has been extensively studied for a long time. Another way to tune the easy direction of magnetization is to introduce rare-earth elements. In that case, the spin–orbit coupling is in competition with the crystal field effect, which leads to a variety of anisotropy, owing to the element involved. Such an effect has been encountered in garnet-type $R_3Fe_5O_{12}$ compounds: $Sm_3Fe_5O_{12}$ and $Er_3Fe_5O_{12}$ display different easy direction of magnetization in agreement with their anisotropy constants, such as $K_1=-0.4$ MJ/m^3, $K_2=0$ MJ/m^3 and $K_1=0.09$ MJ/m^3, $K_2=0.5$ MJ/m^3, respectively [15].

The present work takes place in a global study of the anisotropy modulation of cobalt-based ferrites by controlling the substitution of iron for rare earth (RE). Numerous studies on partial substitution of Fe or Co for nonrare earth elements (e.g. Ga, Zn, Mn, Al, Cu, etc....) have been undertaken ([16–19] and references therein). Drastic evolutions of the physical properties such as the Curie temperature, Kerr effect, electrical and magnetoresistance properties have been observed. However, the synthesis of pure phases seems to be a difficult task because of the difference in cation sizes. Some peaks attributed to rare earth oxide are often evidenced in the X-ray diffraction patterns [20]. Moreover, no studies have been undertaken on the limit of substitution of iron for a rare-earth ion and most of studies have

* Corresponding author. Fax: +33 3 88 10 72 47.
E-mail address: christophe.lefevre@ipcms.u-strasbg.fr (C. Lefevre).

0022-4596/$ - see front matter © 2010 Elsevier Inc. All rights reserved.
doi:10.1016/j.jssc.2010.09.004

been devoted to weak rare-earth amounts. Ben Tahar et al. [21] and Kahn et al. [22] have studied $CoFe_{1.9}R_{0.1}O_4$ and $CoFe_{1.88}R_{0.12}O_4$ (R=La–Ho) nanoparticles synthesized by forced hydrolysis in polyol and micellar route. Due to the small size of the particles, superparamagnetic relaxation phenomena have been observed. Nevertheless, the authors have concluded that the Fe substitution for RE elements modulates the magnetic properties in a rather complicated way.

In this paper, our interest is focused on the Fe substitution for Sc, considered as a related RE element, in cobalt ferrite. Indeed, chemistry of Sc shows close similarities with chemistry of RE because they have analogous electronic configuration: ($3d^14s^2$) for Sc and ($5d^16s^2$) for the lanthanides. Then in many respects, Sc can be treated as 'prototype', sharing all the properties of the lanthanides that are not dependent upon the 4*f* electrons. Moreover, scandium ion is the smallest among the trivalent RE cations or related ones suggesting that in that case, the substitution could be more easily achieved. Finally, Sc^{3+} is diamagnetic. Substitution of iron for scandium leads then to a simple dilution of the magnetic iron cation and therefore to a modification of magnetic couplings and behaviors.

2. Experimental

$FeCl_3 \cdot 6H_2O$, $CoCl_2 \cdot 6H_2O$ and Sc_2O_3 (99% Alfa Aeasar, 99% Alfa Aeasar and 99.99% Alfa Aesar, respectively) taken in the following stoichiometric ratios $2-r$, 1 and $r/2$, respectively, ($0 \le r \le 1$) were dissolved in hydrochloric acid (Carlo Erba Reagenti). The solution was then added drop by drop into a 14 M boiling KOH solution. The resulting precipitate was left to boil for 30 min in order to favor the Ostwald ripening. It was then filtered, washed with hot water until no more Cl^- was detected, and annealed at 600 °C under air for 24 h. The resulting powder was manually ground. An organic binder (polyvinyl alcohol) was systematically added at around 3 wt% to improve the mechanical behavior of the samples. The powders were finally compacted into pellets and sintered in a platinum crucible at 1200 °C for 12 h under air.

The powders have been characterized by the X-ray powder diffraction by using a Siemens D8 diffractometer equipped with a Cu $K\alpha_1$ radiation (λ=1.54056 Å) and a Sol-X detector in the 2θ (°) range 27–65° with a scan step of 0.02°. The lattice parameters were refined by least square procedure. Lattice strains were analyzed by using the properties of the Fourier transform [23] from the (113) and (104) reflexions and a scan step acquisition of 0.005°. A correction of the instrumental broadening has been performed with corundum as standard. Samples with low scandium content were also checked by scanning electron microscopy (SEM) using a JEOL electron microscope 6700 coupled with EDX spectroscopy.

Magnetic characterizations were obtained using a vibrating-sample magnetometer equipped with an external field up to 1.8 T for the $M=f(H)$ isothermal curves and using a MANICS magneto-susceptometer in the temperature range 300–850 K for the $M=f(T)$ isofield curves. The Curie temperatures have been defined as the temperatures at which $|dM/dT|$ is maximum.

Zero-field ^{57}Fe Mössbauer measurements were carried out at 300 and 77 K in a transmission mode with constant acceleration using a ^{57}Co/Rh γ–ray source. In-field Mössbauer spectra up to B_{app}=8 T were collected for r=0.1 and r=0.2 at T=10 K. Measurements have been made using a cryomagnetic device which generates an external magnetic field oriented parallel to the γ-beam. The spectrometer was previously calibrated using a standard α-Fe foil and the isomer shift values were expressed with respect to this standard. The fitting of the spectrum was performed using the MOSFIT [24] program with magnetic components composed of lorentzian lines.

3. Results

3.1. X-ray diffraction and SEM observations

The X-ray diffraction patterns exhibit the peaks characteristic of AB_2O_4 spinel structure (space group SG *Fd*-3*m*, no. 227) (Fig. 1). For $r \ge 0.4$, the main diffraction peaks (222) of Sc_2O_3 (SG *Ia*-3 no. 206) appears at $2\theta \approx 31°$ and its intensity increases for increasing amounts of scandium. The scandium ratio in the spinel phase is lower than r. The spinel phase is therefore labeled $CoFe_{2-x}Sc_xO_4$ in the following. With increasing r value, the spinel diffraction lines are shifted towards the low values of 2θ, indicating an increase of the cell parameter (Fig. 2 and Table 1). The lattice parameter calculated for r=0 is equal to 0.8390(1) nm in agreement with the value commonly found for $CoFe_2O_4$ and follows a quasi-linear variation for values of r up to 0.3. Between r=0.3 and 0.4, the lattice parameter is constant. For $r > 0.4$, the variation is again quasi-linear, but with a lower slope. In the high Sc concentration range (r=1), a drastic reduction of the cell parameter is observed. Finally for $r > 1$, some weak additional lines appear in the X-ray diffraction pattern in addition to the spinel structure and the scandium oxide, Sc_2O_3. But they are not quite well defined for further investigations. SEM observations show no impurities for $r < 0.3$. EDX analysis on the r=0.3 sample display small amount of Sc_2O_3 in the powder. This impurity is not observed by the X-ray diffraction due to its small quantity lower than the XRD detection limit.

3.2. Magnetic properties

The magnetic hysteresis loops and particularly saturation magnetization M_s also depict the substitution of iron for scandium (Fig. 3). M_s decreases from 3.52 μ_B/f.u. (84 emu/g) for $CoFe_2O_4$ down to 2.17 μ_B/f.u. (49 emu/g) for $CoFe_{1.8}Sc_{0.2}O_4$. For higher scandium content, the additional diamagnetic phase Sc_2O_3 also contributes to the decrease of the magnetization, due to the

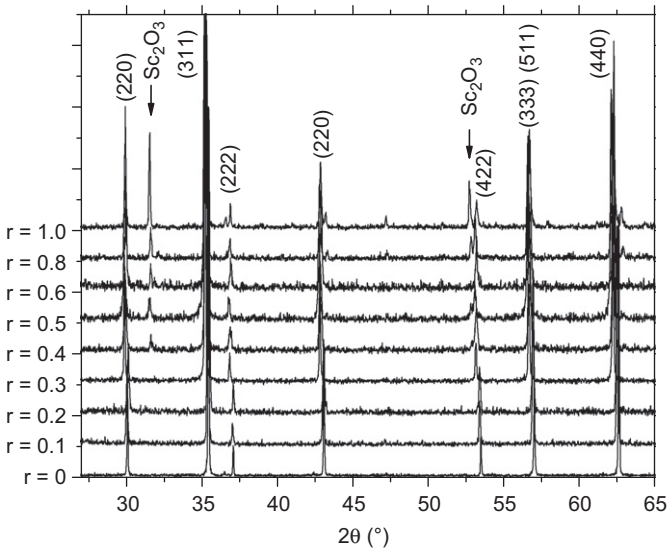

Fig. 1. X-ray diffraction patterns recorded at room temperature on $CoFe_{2-r}Sc_rO_4$ series ($0 \le r \le 1$). The indexation is performed according to the $CoFe_2O_4$ spinel phase (JCPDS #221086 [40]).

overestimation of the weight of the spinel phase. The coercive field increases from H_C=1200 G for r=0 up to H_C=7194 G for r=0.8 as shown in Table 1. The thermal variation of the magnetization under an applied field H=0.1 T shows that the Curie temperature decreases with the increase of scandium concentration from T_C=792 K for $CoFe_2O_4$ (i.e. r=0) to T_C=512 K for r=1 (Fig. 4).

3.3. Mössbauer spectrometry

Zero-field Mössbauer spectra recorded at 77 and 300 K on the different compositions are depicted in Fig. 5. At room temperature and except for r=0.8, each recorded spectrum consists of sextets characteristic of magnetic ordering. The r=0.8 spectrum exhibits an important quadrupolar contribution characterized by a large doublet which is representative of a paramagnetic state of clusters of iron atoms. Results of the refinements performed at 77 and 300 K are listed in Tables 3a and b, respectively. Refined values of the isomer shift for all samples are consistent with high spin state Fe^{3+} ions either in tetrahedral site or in octahedral site. No Fe^{2+} is detected. The lack of resolution of the magnetic hyperfine structure prevents from a clear quantitative description in terms of both tetrahedral and octahedral Fe sites. The distribution can be accurately determined providing an external magnetic field has to be applied on the sample as they do exhibit a ferrimagnetic structure. Indeed, the in-field Mössbauer spectra recorded at 10 K on the r=0.1 and r=0.2 compositions and illustrated in Fig. 6, clearly show the presence of two kinds of magnetic sextets, the line intensities of which strongly differ from that of random magnetic powder. Substitution of Fe for Sc involves a variety of surroundings that can be described considering several components characterized by different values of hyperfine parameters. However, these different components are purely mathematical and then only the mean values of the hyperfine parameters for both sites have been reported in Table 4. Canting effect is observed for r=0.1 whereas the second line intensity decreases for r=0.2 showing that canting effect is very small for the tetrahedral site for this composition ($\beta < 10^\circ$). This effect comes probably in the fact that substitution of iron for a nonmagnetic element (Sc) changes the environment of the T_d sites decreasing the magnetic interactions. The direct consequence is a diminution of the frustration between T_d and O_h sites.

The refinement of the in-field Mössbauer spectra allows also to estimate the ratio between Fe^{3+} atoms located in tetrahedral and

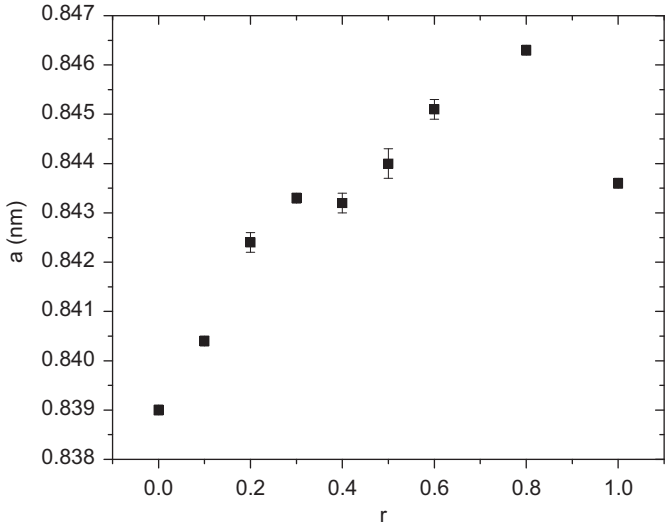

Fig. 2. Variation of the lattice parameter of the observed spinel phase versus r for $CoFe_{2-x}Sc_xO_4$.

Table 2
Metal–oxygen distance in tetrahedral (α) and octahedral (β) sites (from [28]).

	α	β
Co^{2+}	1.967	2.126
Co^{3+}	–	1.893
Fe^{3+}	1.858	2.02
Sc^{3+}	–	2.172

Table 1
Nominal compositions r, refined lattice parameters a, calculated composition x, inversion parameter s, Co^{3+} content in the$(Fe_s^{3+}Co_{1-s}^{2+})[Co_s^{2+}Co_\delta^{3+}Fe_{1-r-\delta-s}^{3+}Sc_r^{3+}]O_4$ spinel phase, cationic distribution, size and strain of the different samples, experimental saturation magnetization, coercive field and Curie temperatures.

r	a (nm)	x	s	δ	Structural formula	Size (nm)[a]	$\langle\varepsilon^2\rangle^{1/2}$ ($\times 10^3$)[b]	M_s (5 K) (μ_B/f.u.)	H_c (5 K) (G)	T_C^c (K)	T_C^e (K)
0	0.8390(1)	0.00(1)	0.88 (1)	0	$(Fe_{0.88}^{3+}Co_{0.12}^{2+})[Co_{0.88}^{2+}Fe_{1.12}^{3+}]O_4$	150	0.56(1)	3.52	1200	780	791
						137	0.40(1)				
0.1	0.8404(1)	0.08(1)	0.98 (1)	0	$(Fe_{0.98}^{3+}Co_{0.02}^{2+})[Co_{0.98}^{2+}Fe_{0.94}^{3+}Sc_{0.08}^{3+}]O_4$	163	0.52(1)	2.73	6500	748	753
						150	0.45(1)				
0.2	0.8424(2)	0.18(2)	0.99 (1)	0	$(Fe_{0.99}^{3+}Co_{0.01}^{2+})[Co_{0.99}^{2+}Fe_{0.83}^{3+}Sc_{0.18}^{3+}]O_4$	154	0.55(1)	2.17	4922	695	713
						141	0.44(1)				
0.3	0.8434(1)	0.25(1)	1	0.01(1)	$(Fe^{3+})[Co^{2+}Co_{0.01}^{3+}Fe_{0.75}^{3+}Sc_{0.25}^{3+}]O_4$	131	0.69(1)	[c]	3305	660	680
						112	0.58(1)				
0.4	0.8432(1)	0.34(1)	1	0.02(1)	$(Fe^{3+})[Co^{2+}Co_{0.02}^{3+}Fe_{0.66}^{3+}Sc_{0.34}^{3+}]O_4$	132	0.68(1)	[c]	4278	643	653
						112	0.53(1)				
0.5	0.8440(3)	0.41(1)	1	0.03(1)	$(Fe^{3+})[Co^{2+}Co_{0.03}^{3+}Fe_{0.59}^{3+}Sc_{0.41}^{3+}]O_4$	95	0.87(1)	[c]	4870	612	629
						88	0.71(1)				
0.6	0.8451(2)	0.48(1)	1	0.05(1)	$(Fe^{3+})[Co^{2+}Co_{0.05}^{3+}Fe_{0.52}^{3+}Sc_{0.48}^{3+}]O_4$	70	1.10(1)	[c]	3984	569	595
						79	0.84(1)				
0.8	0.8463(1)	0.58(1)	1	0.10(2)	$(Fe^{3+})[Co^{2+}Co_{0.1}^{3+}Fe_{0.42}^{3+}Sc_{0.58}^{3+}]O_4$	90	0.91(1)	[c]	6418	496	524
						77	0.80(1)				
1.0	0.8436(1)	0.56(2)	1	0.22(2)	$(Fe^{3+})[Co^{2+}Co_{0.22}^{3+}Fe_{0.44}^{3+}Sc_{0.56}^{3+}]O_4$	80	1.07(1)	[c]	7194	462	512
						66	0.96(1)				

[a] Using the initial Fourier slope of the (331) plan and the log-normal distribution.
[b] Using the (331) and the (400) plans, respectively.
[c] Not reported (cf. text).

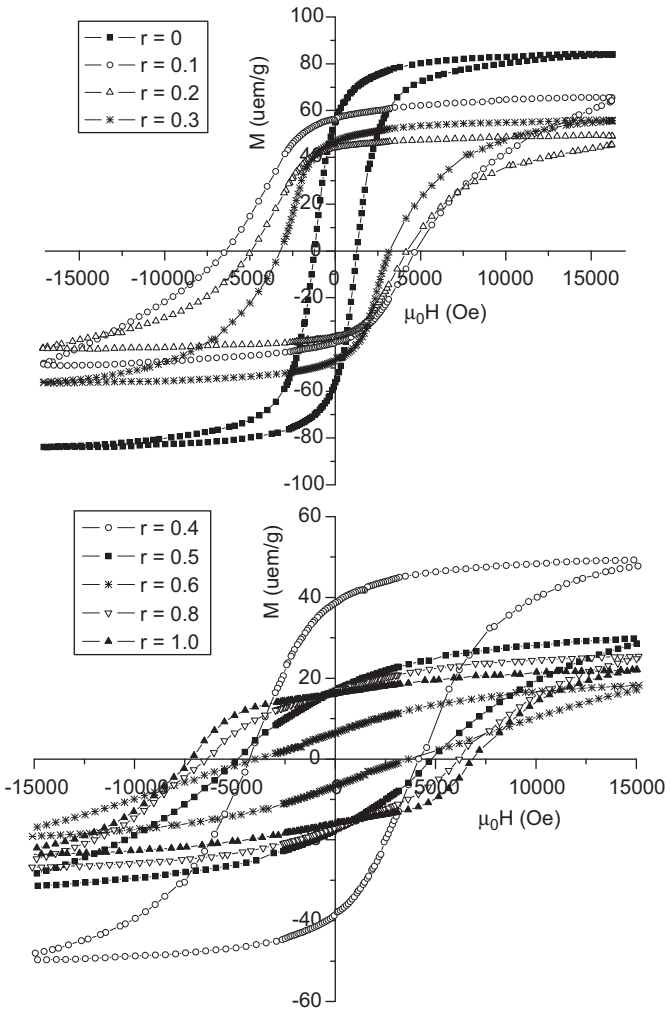

Fig. 3. Hysteresis loop of the $CoFe_{2-r}Sc_rO_4$ ($0 \le r \le 1$) series at 5 K.

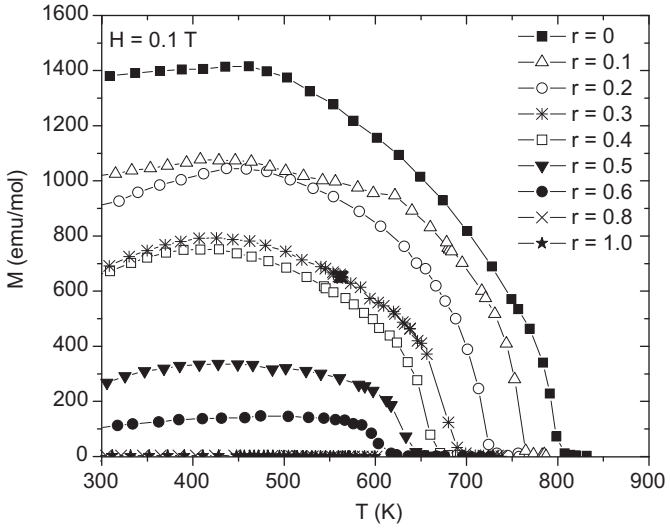

Fig. 4. Thermal variation of the magnetization of the $CoFe_{2-r}Sc_rO_4$ series ($0 \le r \le 1$) in an $H=0.1$ T applied field.

octahedral positions following the relationship:

$$\frac{A_{Td}}{A_{Oh}} = \frac{[\mathrm{Fe}]_{Td}}{[\mathrm{Fe}]_{Oh}}$$

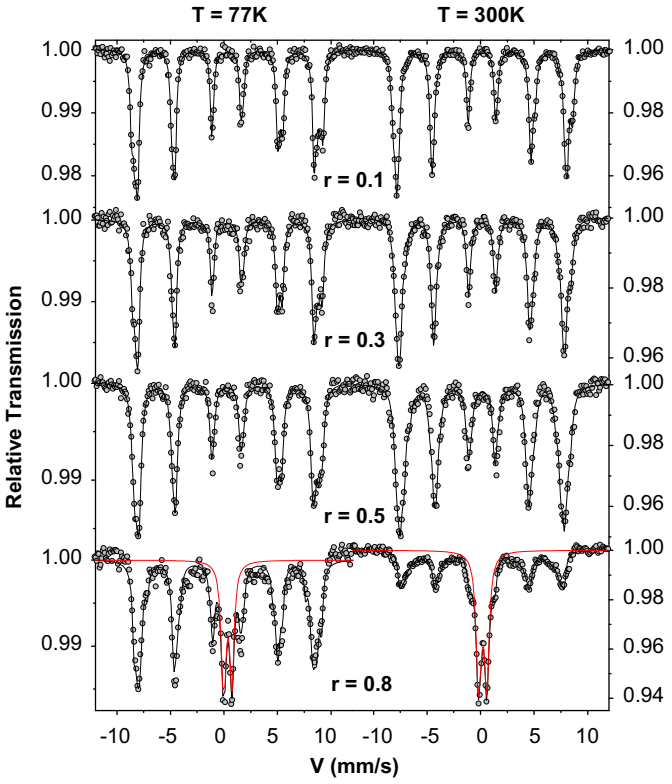

Fig. 5. Mössbauer spectra of the $CoFe_{2-r}Sc_rO_4$ ($0 \le r \le 1$) series recorded at 77 K (left) and 300 K (right).

Table 3
Average Mössbauer hyperfine parameters extracted from refinements of (a) 77 K and (b) 300 K spectra. δ is the isomer shift, 2ε is the quadrupolar shift and B_{hyp} is the hyperfine field.

	$\langle\delta\rangle$ (mm/s)	$\langle 2\varepsilon\rangle$ (mm/s)	$\langle B_{hyp}\rangle$ (T)
(a) 77 K			
$x=0.1$	0.43(1)	−0.02(1)	52.7(1)
$x=0.2$	0.43(1)	−0.01(1)	52.6(1)
$x=0.3$	0.43(1)	−0.02(2)	52.3(1)
$x=0.4$	0.44(1)	−0.00(2)	52.0(1)
$x=0.5$	0.44(1)	0.00(2)	51.8(1)
$x=0.6$	0.44(1)	−0.02(2)	51.1(1)
$x=0.8$	0.44(1)	−0.02(3)	50.4(1)
	0.50(1)	0.72(1)	0
(b) 300 K			
$x=0.1$	0.29(1)	−0.01(1)	49.4(1)
$x=0.2$	0.32(1)	0.02(2)	48.7(1)
$x=0.3$	0.32(1)	−0.00(2)	47.9(1)
$x=0.4$	0.32(1)	0.00(1)	47.4(1)
$x=0.5$	0.33(2)	0.00(3)	47.1(1)
$x=0.6$	0.32(1)	0.03(2)	45.7(1)
$x=0.8$	0.36(1)	0.69(5)	0
	0.31(1)	−0.02(1)	42.1(1)

assuming that the ratio of the recoilless fractions $f_B/f_A=1$ at low temperature. We calculate $[Fe]_{Td}/[Fe]_{Oh}=0.66(5)$ for $r=0.1$ and $[Fe]_{Td}/[Fe]_{Oh}=0.75(6)$ for $r=0.2$.

4. Discussion

The lattice parameter as well as both the saturation magnetization and the Curie temperature are dependent on the cationic distribution within the spinel structure. The spinel structure can be described as a close packed fcc arrangement of 32 oxygen

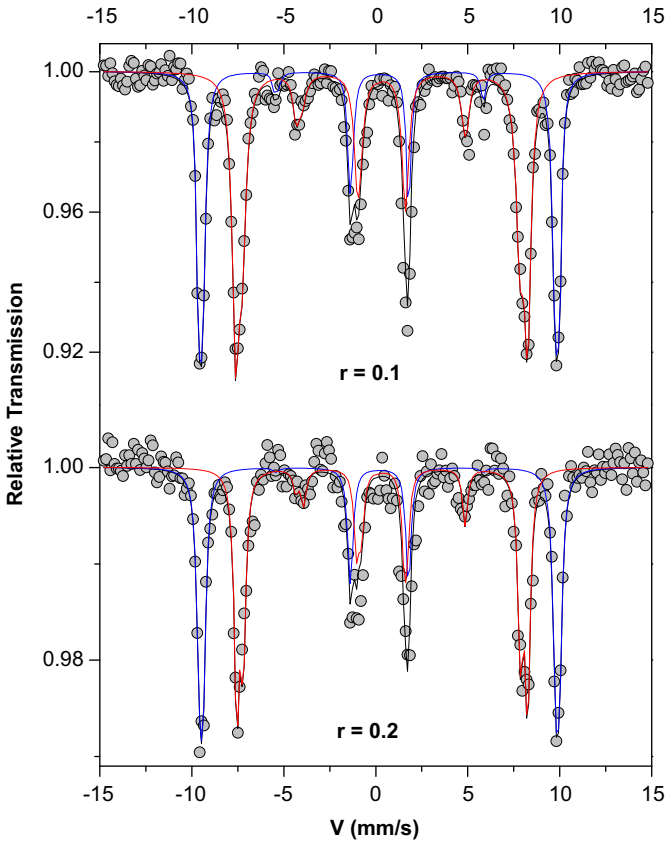

Fig. 6. In-field Mössbauer spectra of $CoFe_{1.9}Sc_{0.1}O_4$ and $CoFe_{1.8}Sc_{0.2}O_4$ recorded at 10 K under a 8 T external field applied parallel to the γ-beam.

Table 4
Mössbauer hyperfine parameters extracted from refinements of the 10 K spectra under an 8 T applied field: isomer shift δ, quadrupolar contribution 2ε, effective hyperfine field B_{eff}, hyperfine field B_{hyp}, canting angle β and subspectra area.

	$\langle\delta\rangle$ (mm/s)	$\langle 2\varepsilon\rangle$ (mm/s)	$\langle B_{eff}\rangle$ (T)	$\langle\beta\rangle$ (deg.)	$\langle B_{hyp}\rangle$ (T)	A (%)
$x=0.1$	0.37(2)	−0.03(3)	60.0(1)	18(2)	52.4(1)	40(2)
	0.51(1)	−0.03(3)	47.9(1)	27(1)	55.1(1)	60(2)
$x=0.2$	0.38(3)	0[a]	59.8(1)	<10	52.2(1)	43(2)
	0.50(1)	−0.01(1)	47.5(1)	25(2)	54.8(1)	57(2)

[a] Fixed value during the fitting procedure.

anions O^{2-} designing 64 tetrahedral (T_d) and 32 octahedral [O_h] sites. One eighth of the T_d sites and half of the O_h sites are occupied. The cationic distribution on the two sites may be written as $(A_{1-s}B_s)[A_sB_{2-s}]O_4$ with s varying between $s=0$ (normal spinel) and $s=1$ (inverse spinel). For the cobalt ferrite compounds, values of s between 0.74 and 0.93 have been reported. They depend on many parameters such as the thermal treatment [25–27]. Sc^{3+} which has a larger ionic radius than that of Fe^{3+} ions ($r_{Fe^{3+}}=0.645$ Å and $r_{Sc^{3+}}=0.745$ Å [28]) is preferentially located in the octahedral site where the volume is the most important. Such a distribution is consistent with the linear increase of the lattice parameter up to $r=0.3$ and with the decrease of the magnetization as the magnetic moments of A and B sites are opposite. Indeed, the magnetic moment of octahedral site is decreased while Sc^{3+} located in the tetrahedral site would result in an increase of magnetization.

Poix [29] has previously shown that the lattice parameter a of spinel compounds can be expressed by:

$$a=2.0995\alpha+\sqrt{5.8182\beta^2-1.4107\alpha^2} \quad (1)$$

where α and β are the average cation-oxygen distances in tetrahedral and octahedral sites, respectively (Table 2). For r values between 0 and 0.2, the formula can be written as $(Fe_s^{3+}Co_{1-s}^{2+})[Co_s^{2+}Fe_{2-x-s}^{3+}Sc_x^{3+}]O_4$, assuming that all the scandium atoms enter the octahedral positions. α and β of Eq. (1) are therefore given by

$$\alpha=s\alpha_{Fe^{3+}}+(1-s)\alpha_{Co^{2+}} \text{ and } \beta=\frac{1}{2}\left[s\beta_{Co^{2+}}+(2-x-s)\beta_{Fe^{3+}}+x\beta_{Sc^{3+}}\right]$$

The saturation magnetization can also be expressed as a function of s and x by

$$M_S=M_{Oh}-M_{Td}=(2s-1)\mu_{Co^{2+}}+(2-x-2s)\mu_{Fe^{3+}}$$

Assuming a total quenching of the orbital moment of the 3d elements, the expression becomes (in μ_B/f.u.)

$$M_S=7-5x-4s \quad (2)$$

For $r\geq 0.3$, the presence of Sc_2O_3 suggests thus that the cell cannot rearrange itself to accept all the scandium ions with the present chemical conditions of synthesis. Assuming that all starting Fe^{3+} and Co^{2+} ions are located into the spinel compounds, justified by the fact that no other Co and Fe based contributions are detected in the X-ray diffractograms, all compounds can be described by formula $CoFe_{2-r}Sc_xO_4$ with $x<r$. Then if we consider Co^{2+}, Fe^{3+} and Sc^{3+}, we have a lack of positive charge into the system. Therefore, in order to satisfy the charge balance within the spinel structure, cobalt is partially oxidized. The formula becomes$(Fe^{3+})[Co^{2+}Co_\delta^{3+}Fe_{1-x-\delta}^{3+}Sc_x^{3+}]O_4$ whereas α and β of Eq. (1) are thus expressed as

$$\alpha=\alpha_{Fe^{3+}} \text{ and } \beta=\frac{1}{2}\left[\beta_{Co^{2+}}+\delta\beta_{Co^{3+}}+(1-x-\delta)\beta_{Fe^{3+}}+x\beta_{Sc^{3+}}\right]$$

the second equation is

$$\frac{[Co]}{[Fe]}=\frac{1}{2-r}=\frac{1+\delta}{2-\delta-x} \quad (3)$$

Using Eq. (2) for $r=0$ and combining Eqs. (1) and (2) for $0.2\geq r\geq 0.1$; (1) and (3) for $r\geq 0.3$ allows the determination of s, δ and x (Table 1). An inversion rate of 0.879(5) for cobalt ferrite ($r=x=0$) is in good agreement with previous results. When r increases up to 0.3, s increases up to 1, i.e. the tetrahedral site contains only iron cations when $r\geq 0.3$. Although this trend corroborates the in-field Mössbauer results, the values of s are slightly different despite the error measurement. Such a disagreement could be explained by the occurrence of spin reverse phenomena and/or the mismodelling of the local disorder by the Poix method. Consequently, further investigations are necessary to clarify this point.

Both δ and x follow a quasi-linear variation in the range $r=0.4$–0.8 (Fig. 7). The amount of Co^{3+} as well as the scandium ratio increases in the spinel phase until the substitution limit is reached for $x\approx 0.5$ ($r=0.8$). Finally, for $r>0.8$, x does not vary anymore and the strong decrease of the cell parameter is associated to an increase of the Co^{3+} content associated to the increase of the deficit of the positive charge in the spinel structure.

The substitution of iron for scandium yields to a strong increase of the strains within the structure and particularly on the O_h sites due to the difference of the ionic radii. Let us analyze the

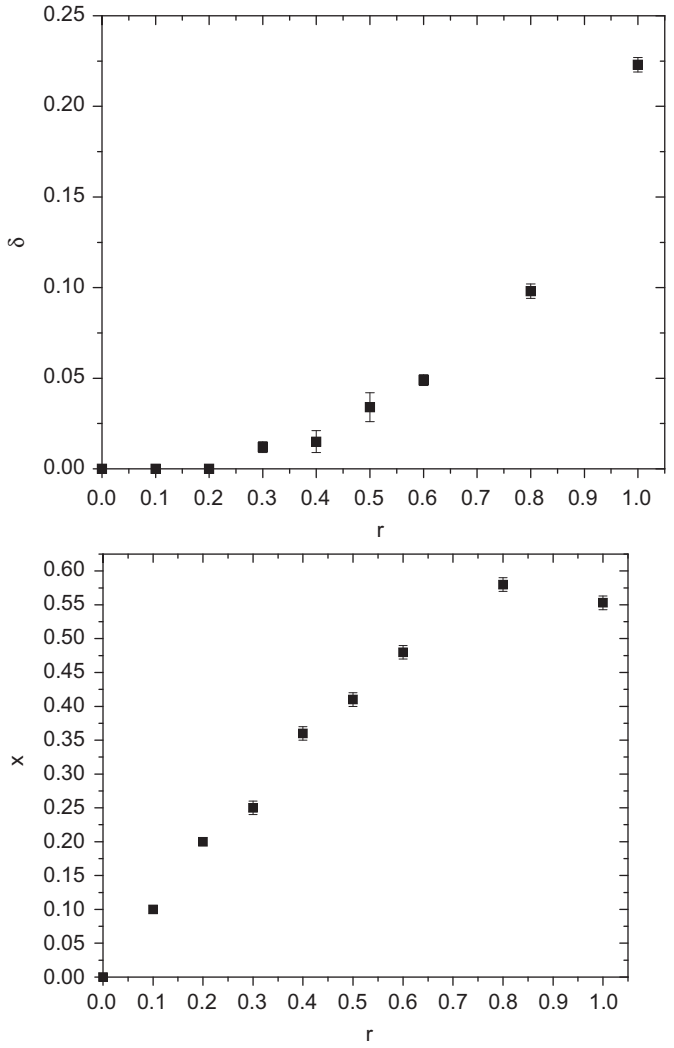

Fig. 7. Evolution of the Co^{3+} content (δ) and the calculated composition (x) with the nominal composition (r).

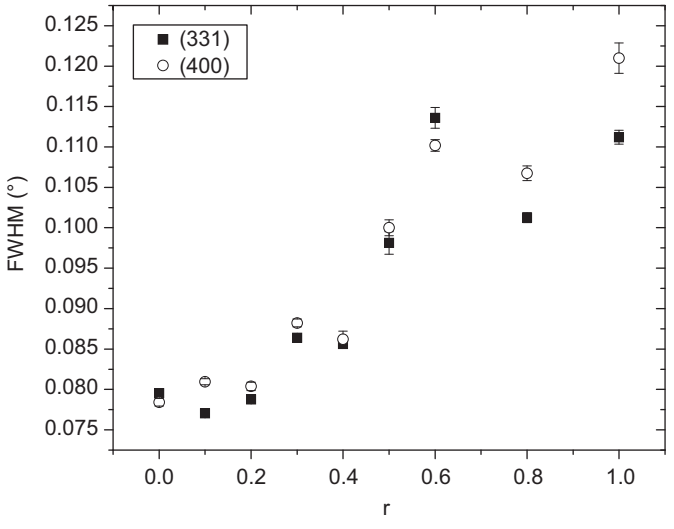

Fig. 8. Variation of the full width at half maximum versus the nominal composition (i.e. r) for the spinel (331) and (400) reflexions. The measurements have been recorded in the range [$\theta_{Bragg}-0.5^\circ$; $\theta_{Bragg}+0.5^\circ$] with a scan step acquisition of 0.005° and a counting time of 16 s/step.

full width at half maximum (FWHM) for the (331) and the (400) reflexions versus x (Fig. 8). FWHM value increases when the scandium content increases, from FWHM=0.079(1)° and 0.078(1)° for the (331) and (400) planes, respectively, for $CoFe_2O_4$ up to FWHM=0.111(1)° and 0.120(1)° for $(Fe^{3+})[Co^{2+}Co^{3+}_{0.22}Fe^{3+}_{0.22}Sc^{3+}_{0.56}]O_4$($r=1$) (Fig. 8). It is well established that three main factors contribute to the FWHM: the instrumentation, the size of the coherent diffracting domain and the strains. After correcting the instrumental broadening, the true profiles have been deconvoluted in order to get information on the strains and the diffracting volume size. According to the Warren–Averbach method [30,31], the cosine Fourier coefficient $A(L)$ of the profiles is expressed as the product of size $A_S(L)$ and strain $A_D(L)$ components following the expression:

$$A(L) = A_S(L)A_D(L) = A_S(L)(1-\exp(-2\pi^2 g^2 L^2 \langle \varepsilon^2_{g,L} \rangle))$$

where g is the absolute value of the diffraction vector, $\langle \varepsilon^2_{g,L} \rangle$ is the mean square strain and L is the Fourier length defined by $L = n\lambda/2(\sin\theta_2 - \sin\theta_1)$ where λ is the wavelength of the X-ray, n is the Fourier harmonic number and $[\theta_1,\theta_2]$ is the profile range of the diffraction line. Plot of Fourier coefficients $A(L)$ as a function of the Fourier length are given in Fig. 9 for the different r compositions. The hook effect observed for small values of L is due to the error in

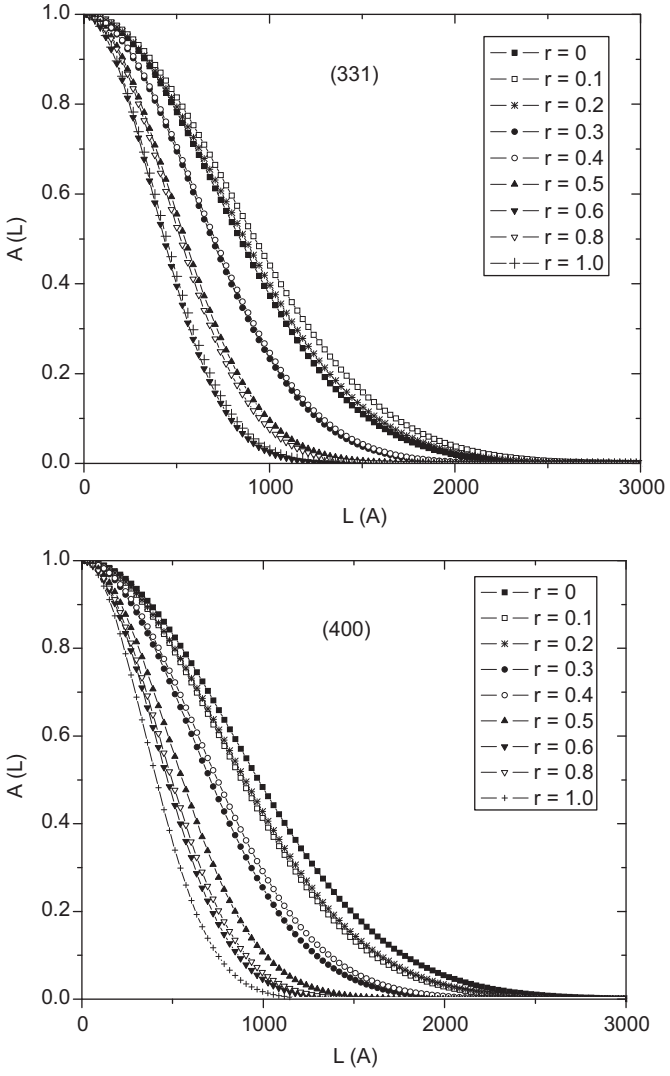

Fig. 9. Evolution of the normalized Fourier coefficient versus the Fourier length of the (331) and (400) plane.

the estimated background and the fact that profiles are necessarily truncated for a finite range. According to Warren, the apparent D_S domain size is given by $(dA_L/dL)_{L\to 0} = -1/D_S$ [30–32]. The sizes are thus related to the intercept of the linear part with the abscissa axis. Size distribution is obtained plotting the second derivate of the Fourier coefficient versus the Fourier length (Fig. 10) [32]. The coherent diffraction domain size is close to 150 nm for $CoFe_2O_4$ ($x=0$) and about 70 nm for the highest scandium ratio ($x=0.55$). The size distribution increases with the Sc content. The strain variation with the scandium content is given in Fig. 11 where the root main square strain $\sqrt{\langle \varepsilon_{g,L}^2 \rangle}$(rmss) is represented versus r. An increase of the rmss with the scandium ratio r in both directions (i.e. [311] and [400]) is observed. This augmentation must be associated to the difference between the Sc^{3+} and Fe^{3+} radii favouring thus stresses in octahedral sites.

Substitution of iron for scandium has also a direct consequence on the magnetic properties. This impact is clearly evidenced regarding the Curie temperature and the hyperfine field (Fig. 4, Tables 1, 3a, b and 4). It is related to a modification of the interactions within the structure [33–35]. Compounds having a B site or an A site occupied only with a nonmagnetic element and then having $J_{AB}=J_{BB}=0$ or $J_{AB}=J_{AA}=0$, respectively, displays a very low Curie temperature (e.g. 8 and 20 K for $FeAl_2O_4$ and $ZnFe_2O_4$, respectively [36,37]), whereas compounds having magnetic elements in both sites exhibit rather a high T_C (e.g. $T_C=713$ K for $Mg_{0.1}Fe_{0.9}[Mg_{0.9}Fe_{0.1}]O_4$ [38]). Identical assumptions have been then done in this paper. According to the Stephenson model based on the Weiss molecular field theory, the Curie temperature of $Fe_s^{3+}Co_{1-s}^{2+}[Sc_x^{3+}Fe_{2-x-s}^{3+}Co_s^{2+}]O_4$ is given by the formula

$$T_C = C_0\left(\frac{8.4}{a}\right)^{13}\sqrt{\frac{2\Delta}{D-\sqrt{D^2-4\Delta}}} \quad \text{if } \Delta \neq 0$$

$$T_C = C_0\left(\frac{8.4}{a}\right)^{13}\sqrt{D} \quad \text{otherwise}$$

where C_0 is a constant depending on the spin quantum number and the molecular field factors; D and Δ are parameters defined by the two relationships: $\Delta = 0.0222s^2(1-s)(2-x-s)$ and $D = s(2-x-s)+0.243(s^2+0.922(1-s)(2-x-s))+0.00709s(1-s)$ [35]. For low scandium concentrations, the Curie temperature can be directly calculated following the previous relation. For $r \geq 0.3$ (i.e. $x \geq 0.24$), a low spin state t_{2g}^6 of Co^{3+} due to a strong octahedral field is considered. Consequently a large crystal field splitting between t_{2g} and e_g allowing to consider Co^{3+} as well as Sc^{3+} as a nonmagnetic element [39]. In that case, $\Delta = 0$ and $D = 1.243-x-\delta$. The calculated T_C^c values versus the experimental values T_C^e are compared in Fig. 12: T_C^c is systematically lower than T_C^e since J_{AA} and J_{BB} have been disregarded. The discrepancy strongly increases at the substitution limit for $r \geq 0.8$.

On increasing the Sc^{3+} concentration, the values of isomer shifts of the T_d and O_h sites do not show any appreciable change (Tables 3a and b). This indicates that the s electron density at the Fe^{3+} nucleus is not affected by Sc^{3+} ion concentration in $CoFe_{2-x}Sc_xO_4$ system. Moreover, the refined hyperfine field values at T_d and O_h sites show a monotonic decrease with increasing scandium substitution. The decrease of the hyperfine field could be explained qualitatively. Indeed an atom A at the T_d site is surrounded by 12 B neighboring sites at the distance $d = a\sqrt{11}/8$ distributed in a regular hexacosaedron. When Sc is substituting Fe at the Oh site, the resulting field which is observed by a $(Fe)_{Td}$ decreases. An atom at the B site is surrounded by six A and B neighboring atoms at distance $d = a\sqrt{11}/8$ and $d = a\sqrt{2}/4$,

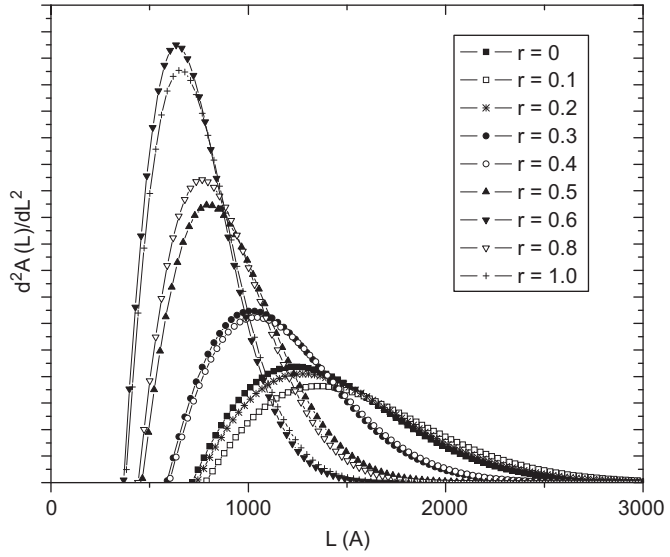

Fig. 10. Evolution of the second derivative of the Fourier coefficient $A(L)$ of the (331) planes versus the Fourier length L.

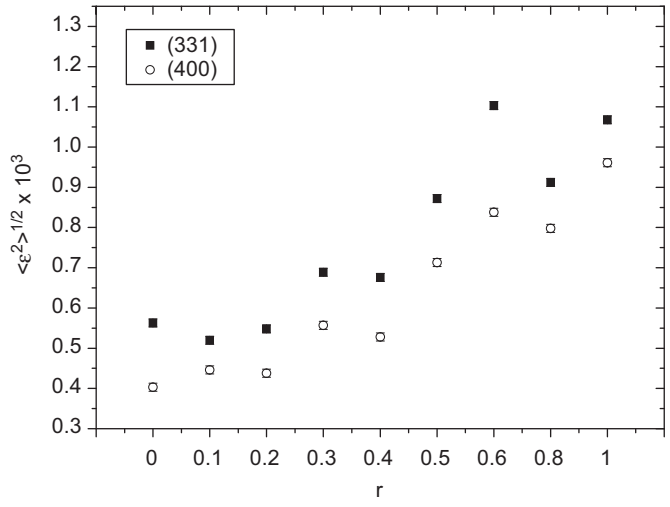

Fig. 11. Evolution of the strains in the (331) and (400) directions versus the nominal composition.

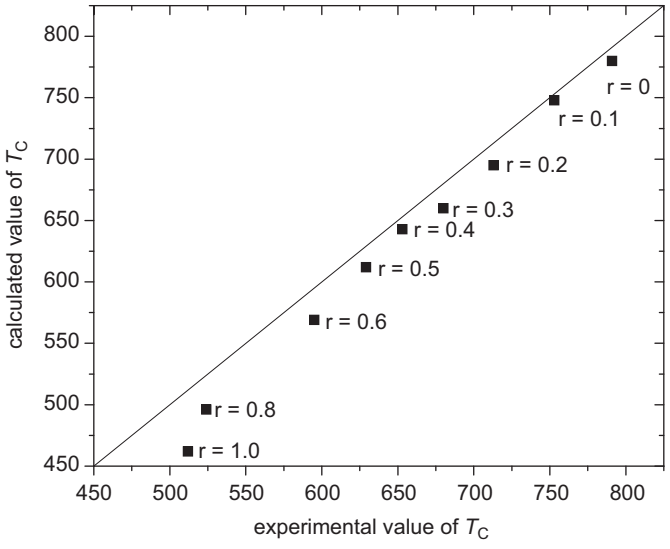

Fig. 12. calculated versus experimental values of T_C of the$CoFe_{2-r}Sc_rO_4$ series ($0 \leq r \leq 1$).

respectively. So, as previously, the Fe^{3+} substitution for Sc^{3+} at the O_h site reduces the hyperfine field which is seen by Fe atoms at the T_d site. Such a feature is probably associated to decreasing superexchange interactions.

5. Conclusions

Using the Poix model, the magnetization at saturation and the chemical content of our phases, the limit of the substitution of iron for scandium in $CoFe_{2-x}Sc_xO_4$ has been determined to be equal to $x=0.56$. The increase of scandium amount is accompanied by an increase of the lattice parameter and of strains, and a diminution of the crystallite size. A ferrimagnetic ordering has been observed for all compositions. The experimental values of T_C are well described by the proposed model which depends mainly on the J_{AB} interaction. Consequently, J_{AB} decreases with the increasing Sc^{3+} content while the two other interactions (J_{AA} and J_{BB}) become less and less negligible. For $x > 0.3$, Co^{3+} is observed, suggesting that for the stabilization of the spinel structure, the RE size must be counterbalanced by the occurrence of a smaller cation. Such a fact must be taken into account for further developments of RE-doped spinel ferrites.

References

[1] N.W. Grimes, Phys. Technol. 6 (1975) 22.
[2] K.E. Sickafus, J.M. Wills, N.W. Grimes, J. Am. Ceram. Soc. 82 (1999) 3279.
[3] G. Amatucci, J.M. Tarascon, J. Electrochem. Soc. 149 (2002) K31–K46.
[4] F. Tihay, A.C. Roger, G. Pourroy, A. Kiennemann, Energy Fuels 16 (2002) 1271.
[5] S. Teja, P.Y. Koh, Prog. Cryst. Growth Charact. Mater. 55 (2009) 22.
[6] M. Veverka, P. Veverka, O. Kaman, A. Lancok, K. Zaveta, E. Pollert, K. Knızek, J. Bohacek, M. Benes, P. Kaspar, E. Duguet, S. Vasseur, Nanotechnology 18 (2007) 345704.
[7] T.J. Daou, J.M. Greneche, G. Pourroy, S. Buathong, A. Derory, C. Ulhaq-Bouillet, B. Donnio, D. Guillon, S. Begin-Colin, Chem. Mater. 20 (2008) 5869.
[8] N.W. Speliotis, J. Appl. Phys. 38 (1967) 1207.
[9] A.E. Berkowitz, W.J. Shuele, P.J. Flanders, J. Appl. Phys. 39 (1968) 1261.
[10] R. Dosoudil, M. Usakova, J. Franek, J. Slama, V. Olah, J. Magn. Magn. Mater. 304 (2006) e755–e757.
[11] M. Pardavi-Horvath, J. Magn. Magn. Mater. 215 (2000) 171.
[12] E. Prince, Phys. Rev. 102 (1956) 674.
[13] K. Yosida (Ed.), Theory of Magnetism, Springer Verlag, 1996.
[14] E.P. Wohlfarth (Ed.), Ferromagnetic Materials, vol. 3, Elsevier Science Publishers B.V, 1982.
[15] R.F. Pearson, J. Appl. Phys. 33 (1962) 1236S.
[16] W.L. Peeters, J.W.D. Martens, J. Appl. Phys. 53 (1982) 8178.
[17] A.K.M. Akther Hossain, H. Tabata, T. Kawai, J. Alloys Compd. 320 (2008) 1157.
[18] J.A. Paulsen, A.P. Ring, C.C.H. Lo, J.E. Snyder, D.C. Jiles, J. Appl. Phys. 97 (2005) 044502.
[19] C. Venkateshwarlu, D. Ravinder, J. Alloys. Compd. 426 (2006) 4.
[20] M.M. Rashad, R.M. Mohamed, H.J. El-Shall, Mat. Proc. Technol. 198 (2008) 139.
[21] L. Ben Tahar, M. Artus, S. Ammar, L.S. Smiri, F. Herbst, M.J. Vaulay, V. Richard, J.M. Grenèche, F. Villain, F. Fievet, J. Magn. Magn. Mater. 320 (2008) 3242.
[22] M.L. Kahn, Z.J. Zhang, Appl. Phys. Lett. 78 (2001) 3651.
[23] A.R. Stockes, Proc. Phys. Soc. London 61 (1948) 382.
[24] J. Teillet, F. Varret, unpublished MOSFIT Program (Université du Maine, Le Mans, France).
[25] L. Néel, C. R. Acad. Sci. 230 (1950) 190.
[26] G.A. Sawatsky, F. Van de Woude, A. Morrish, Phys. Rev. 187 (1969) 747.
[27] M.R. De Guire, R.C. O'Handley, G. Kalonji, J. Appl. Phys. 65 (1989) 3167.
[28] R.D. Shannon, C.T. Prewitt, Acta Cryst. B 25 (1969) 925.
[29] P. Poix, Bull. Soc. Chim. Fr. 2 (1965) 1085.
[30] B.E. Warren, in: X-ray diffraction, Addison-Wesley, New York, 1970.
[31] B.E. Warren, B.L. Averbach, J. Appl. Phys. 21 (1950) 595.
[32] B.E. Warren, in: X-ray diffraction, Dover, New York, 1969.
[33] S. Krupicka, P. Novak, in: E.P. Wohlfarth (Ed.), Ferromagnetic Materials, Vol III, North-Holland, Amsterdam, 1987.
[34] P.G. Bercoff, H.R. Bertorello, J. Magn. Magn. Mater. 169 (1997) 314.
[35] A. Stephenson, Phil. Mag. 25 (1972) 1213.
[36] W.L. Roth, J. Phys. Rad. 25 (1964) 507.
[37] U. König, E.F. Bertaut, Y. Gros, M. Mitrikov, G. Chol, Solid State Commun. 8 (1970) 759.
[38] J. Smit, H.P.J. Wijn, Ferrites, Philips' Technical Library, (1959).
[39] W.L. Roth, J. Phys. Chem. Solids 25 (1964) 1.
[40] Natl. Bur. Stand (US) Monogr. 25 (1971) 22.